Available online at www.sciencedirect.com
ScienceDirect
Journal of the European Ceramic Society 27 (2007) 4499–4507
www.elsevier.com/locate/jeurceramsoc

A- and B-compensated PLZT *x*/90/10: Sintering and microstructural analysis

Danjela Kuscer [a,*], Joanna Korzekwa [b], Marija Kosec [a], Ryszard Skulski [b]

[a] *Jožef Stefan Institute, Electronic Ceramics Department, Jamova 39, 1000 Ljubljana, Slovenia*
[b] *University of Silesia, Faculty of Computer Science and Materials Science, Sniezna 2, 41-200 Sosnowiec, Poland*

Received 23 March 2007; accepted 20 April 2007
Available online 31 August 2007

Abstract

Structure–property relationship has been performed in the lanthanum-modified lead–zirconate–titanate (PLZT) with a lanthanum content of 6 and 10 at.% and a Zr/Ti ratio of 90/10 as a function of A- and B-compensation model. The X-ray powder-diffraction analysis, electron microscopy, energy-dispersive spectroscopy, density measurements and sintering behavior have evidently demonstrated that it is possible to tailor the microstructural properties of PLZT with using selected type of the compensation. The densification of B-site compensated PLZT occurs at lower temperatures and leads to higher density when compared to A-site compensated PLZT. A presence of PbO at the grain boundaries in B-site compensated PLZT and the lack of it in A-site compensated PLZT leads to different sintering mechanism. The dielectric response characteristics of A- and B-site compensation model do not vary significantly.

Keywords: Sintering; Grain boundaries; Dielectric properties; PLZT; Perovskites

1. Introduction

Lead-based perovskites are widely used for various devices in the microelectronics industry because of their unique dielectric, piezoelectric and electro-optic properties. Antiferroelectric materials exhibit a field-induced antiferroelectric–ferroelectric phase transformation that produces a larger strain or displacement than ferroelectric materials. This characteristic makes the antiferroelectric materials more attractive for displacement-based micro-electro-mechanical systems.

Zirconium-rich lead–lanthanum–zirconate titanate (denoted PLZT) with the compositions close to $PbZrO_3$ has been reported to exhibit antiferroelectric behavior.[1] Since the trivalent La^{3+} ions are incorporated into the divalent Pb^{2+} sites, the excess charge is compensated by the formation of vacancies, either in the Pb sublattice (A-site vacancies) and/or in the Ti, Zr sublattice (B-site vacancies).[2,3] If the charge compensation occurs exclusively with the formation of A- and B-site vacancies, PLZT is written with the general formulas $Pb_{1-3x/2}La_x(Zr_yTi_{1-y})O_3$ and $Pb_{1-x}La_x(Zr_yTi_{1-y})_{1-1x/4}O_3$, respectively. Holman[3] determined the defect structure of 8/65/35 PLZT using the Knudsen-effusion method. He showed that the continuous effusion of the volatile oxide introduces a linear mass-loss, establishes the concentration of the volatile oxide component within the single-phase sample and allows a description of the sample's defect structure. The experiment eliminated several defect models, and demonstrated that La^{3+} substitutes completely on the Pb^{2+} sublattice, with the charge neutrality requirements satisfied by forming both Pb^{2+} and Zr^{4+}, Ti^{4+} sublattice vacancies.

The vacancy distribution between the A and B sites is affected by the Zr/Ti ratio, the lanthanum content, and the partial pressure of PbO.[2,4,5,6] The formation of the A-site vacancies has been shown to be the key mechanism for accommodating the PbO deficiency in PLZT[7,8]; the A-site vacancies can be formed predominantly at a low partial pressure of PbO. With increasing PbO partial pressure the number of A-site vacancies decreases together with an increasing number of B-site vacancies.[9] It has also been reported that the number of B-site vacancies decreases with increasing ZrO_2 content.[2,6] However, the partial pressure of PbO cannot be increased arbitrarily; it is limited by the condensation of PbO. Other reports suggest that un-reacted PbO either

* Corresponding author. Tel.: +386 1477 3489; fax: +386 1477 3887.
E-mail address: danjela.kuscer@ijs.si (D. Kuscer).

0955-2219/$ – see front matter © 2007 Elsevier Ltd. All rights reserved.
doi:10.1016/j.jeurceramsoc.2007.04.014

sublimates and/or segregates at the grain boundaries during the high-temperature processing of lead-based materials.[10–12] The information available in the literature regarding the compensation of the excess PbO in lead-based perovskites is rather inconsistent. Nevertheless, it is accepted that the properties of lead-based materials depend on the amount of this excess. Polli et al.[13] suggested that the excess PbO is incorporated into the perovskite structure, but to the best of our knowledge the proposed models have not yet been proved.

The reaction sequences for the formation of a PZT solid solution from the corresponding oxides are not completed below 1100 °C.[14] The reactions are as follows. In the first step $PbTiO_3$ is formed at 500 °C, which upon heating reacts with ZrO_2 and PbO, forming various Zr-rich solid solutions. In the next step they react with $PbTiO_3$, forming PZT.[14–18] However, the processing of lead-based ceramics is affected by the relatively high vapor pressure of PbO.[6] The sublimation of PbO during high-temperature processing leads to a change in the PZT stoichiometry, and with higher PbO losses, to the formation of ZrO_2-based secondary phases, as demonstrated in the TiO_2–ZrO_2–PbO phase diagram.[19] The vapor pressure of PbO in a two-phase mixture of PbO and PZT with a defined Zr/Ti ratio depends on the amount of PbO and is not constant.[20,21] Optimization of the processing parameters for lead-based perovskites is very important. Compositional fluctuations in the form of lanthanum-rich regions were reported for PLZT thick films when fired at 1050 °C; however, when fired at 1150 °C the homogeneity and the dielectric and ferroelectric characteristics of PLZT increase significantly.[22]

The densification of PLZT is influenced not only by the temperature and the atmosphere used during the sintering, but also by the amount of PbO present in the initial powder mixture.[23,24] Attempts have been made to fabricate transparent PLZT, and for this the sintering conditions were fully optimized. With a suitable crucible configuration, using the appropriate amount of excess PbO, together with careful control of the atmosphere and the time of sintering, the right conditions to control the microstructure of PLZT can be found.[10,11,20,25,26,27] In order to prepare transparent PLZT, sintering in an oxygen atmosphere with excess PbO was performed first, to obtain fully dense ceramics. In the presence of excess PbO, a PbO-rich liquid phase segregates at the grain boundaries and their existence results in rapid densification of the ceramic.[21,23,28] In the second stage, sintering was performed in air to eliminate the PbO from the grain boundaries, which results in a single-phase microstructure without any pores or PbO phase. Using this procedure, optically transparent ceramics have been produced.

It has been reported that PLZT with the composition 6/90/10 is an antiferroelectric phase with an orthorhombic unit cell.[29] However, the results are rather inconsistent for PLZT 10/90/10. According to the PLZT phase diagram published by Heartling[30] it should be a mixture of orthorhombic PLZT and pyrochlore $La_2Zr_2O_7$. Breval et al.,[29] in their phase diagram, reported that 10/90/10 lies on a line between the antiferroelectric orthorhombic and the mixed-phase regions. The characteristic of the antiferroelectric material is a double hysteresis loop, which was observed for various PZTs with a Zr/Ti ratio from 80/20 to 55/45[1] as well as for antiferreoelectric PLZT 2/95/5.[31] To the best of our knowledge there is no published permittivity data on 6/90/10 nor on 10/90/10 PLZT. A dielectric permittivity of 6400 at a maximum temperature of 210 °C is reported for the antiferroelectric PLZT phase with the composition 2/95/5.[32]

The information regarding the A- or B- compensation models in PLZT available in the open literature is scattered and the fundamental question what is the influence of excess charge in PLZT, which originates from the addition of La^{3+} to the Pb^{2+} crystallographic sites, on the sintering behavior and microstructure, remain. The authors would like to stress that various authors have prepared either A- or B-compensated PLZT at various processing conditions therefore it is unlikely to compare the microstructural characteristics of PLZT prepared at non-identical sintering temperatures, times or atmospheres. In this study we have concentrated at the processing and the structural, microstructural and functional properties of PLZT, assuming that the charge neutrality occurs first, exclusively by A-site vacancy formation, and second, exclusively by B-site vacancy formation. In order to do this we have homogenized raw materials corresponding to the A-site stoichiometry, i.e., $Pb_{1-3x/2}La_x(Zr_yTi_{1-y})O_3$ and to the B-site stoichiometry, i.e., $Pb_{1-x}La_x(Zr_yTi_{1-y})_{1-x/4}O_3$ with $x = 0.06$ and 0.10, and $y = 0.9$, followed by processing the ceramics under identical experimental conditions with careful control of the temperature, time and atmosphere. This paper will focus on sintering process, structural and microstructural characteristics and on the properties of the A- and B-compensated powders prepared at identical experimental conditions. The key differences of A- and B-compensated PLZT will be discussed.

2. Experimental

The PLZT powders chosen for the study, with the compositions A6/90/10, A10/90/10, B6/90/10 and B10/90/10, are shown in Table 1. They were prepared from stoichiometric mixtures of PbO (99.9+% Aldrich, Germany), ZrO_2 (99% Tosoh, Japan), TiO_2 (99.8% Alfa Aesar, Germany) and $La(OH)_3$. The $La(OH)_3$ was prepared from 99.99% La_2O_3 (Alfa Aesar, Germany) by equilibrating it in a humid atmosphere. The starting powders were homogenized in a planetary mill at 200 rpm for 2 h. After drying, the mixtures were calcined at 900 °C for 2 h, re-milled and re-calcined. After a second calcination the powders were milled in an attritor mill and dried.

In order to prepare ceramic pellets the powders were hydraulically uniaxially pressed under 100 MPa pressure and additionally isostatically pressed under 500 MPa. The PLZT compacts were then put in an alumina crucible, covered with

Table 1
Composition of the starting PLZT powders

PLZT composition	La (at.%)	Zr (at.%)	Denoted
$(Pb_{0.91}La_{0.06})(Zr_{0.9}Ti_{0.1})O_3$	6	10	A6/90/10
$(Pb_{0.85}La_{0.10})(Zr_{0.9}Ti_{0.1})O_3$	10	10	A10/90/10
$(Pb_{0.94}La_{0.06})(Zr_{0.9}Ti_{0.1})_{0.985}O_3$	6	10	B6/90/10
$(Pb_{0.90}La_{0.10})(Zr_{0.9}Ti_{0.1})_{0.975}O_3$	10	10	B10/90/10

a powder of an identical composition to the compacts and then sintered at 1200 °C for 1h in the oxygen atmosphere of a closed alumina crucible. The bulk densities of the sintered PLZT pellets were calculated by two independent routs. First, geometrical density was calculated from the mass and the volume of the strictly dimensional uniform pellets. Second, the density was calculated by quantitative characterisation of the ceramic microstructure using computerised image analysis software ImageTools 3.0 (The University of Texas Health Science Center in San Antonio, USA). The binary image obtained from the original micrograph is used to determine the quantity of the pores. Granulometric analyses of the milled powders were performed on a Cilas Hr-850-B laser granulometer from Alcatel.

The sintering behavior of the calcinated PLZT powders was followed using a heating-stage microscope (Leitz Wetzlar, Germany) in the temperature range from 25 to 1400 °C in an oxygen atmosphere.

X-ray powder-diffraction data (XRD) of the sintered A6/90/10, A10/90/10, B6/90/10 and B10/90/10 samples were collected at room temperature on a diffractometer (Endeavor Bruker AXS, Model D4, Karlsruhe, Germany) using Cu Kα radiation. The data were collected in the 2θ range from 20° to 70° in steps of 0.02 degrees with an integration time of 2 s/step. The peak positions and the relative heights of the peaks were determined from the experimental patterns after filtering the Cu $K\alpha_2$ radiation component. The presented phases were identified using the PDF-2[33] database. The lattice parameters of the PLZT were calculated on the basis of an orthorhombic unit cell, as proposed by Breval et al.,[29] using the Topas R (Bruker AXS, Karlsruhe, Germany) software package.

A scanning electron microscope (SEM; Jeol 5800, Japan), equipped with a Tracor Northern energy-dispersive system (EDS) was used for the microstructural analysis. For the SEM analysis the sintered pellets were mounted in epoxy resin in a cross-sectional orientation and polished using standard metallographic techniques. Prior to the SEM/EDS analyses the samples were coated with carbon to provide electrical conductivity and to avoid any charging effects.

The dielectric permittivity as a function of temperature was measured with an HP4192A LF impedance analyzer from Hewlett Packard in the frequency range from 1 kHz up to 1000 kHz for temperatures from 20 to 300 °C. The heating rate was 1–2 °C/min. For the electrical measurements, sintered pellets with a thickness of 0.3–0.4 mm were prepared. The stress was removed by annealing the pellets at 600 °C and then cooling slowly. The surfaces of the pellets were covered on both sides using sputtered gold electrodes (5 Pascal, Italy).

3. Results and discussion

The particle size distributions of the calcined PLZT powders A6/90/10, B6/90/10, A10/90/10 and B10/90/10 are shown in Fig. 1. The median particle size of PLZT A6/90/10 was 0.82 μm, for B6/90/10 it was 0.8 μm, for A10/90/10 it was 0.76 μm, and for B10/90/10 it was 0.97 μm. For PLZT A6/90/10, B6/90/10

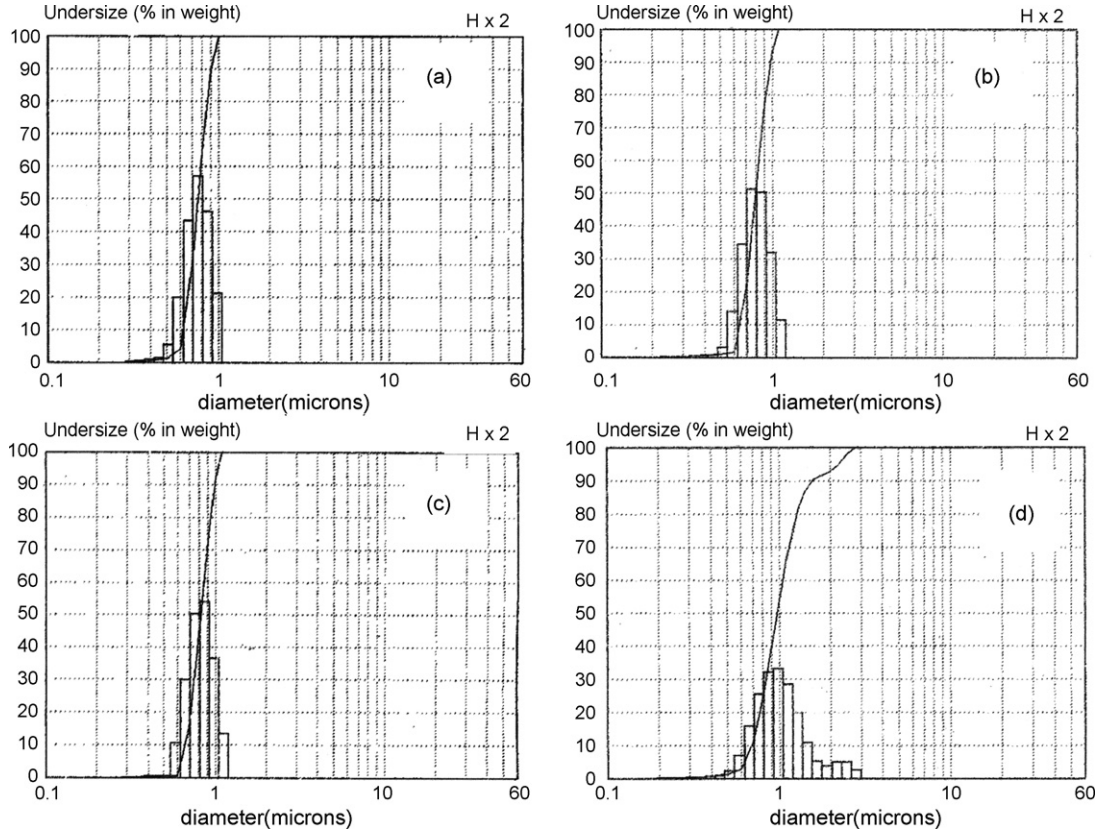

Fig. 1. The particle size distribution of PLZT powder calcined at 900 °C. (a) A6/90/10, (b) B6/90/10, (c) A10/90/10 and (d) B10/90/10.

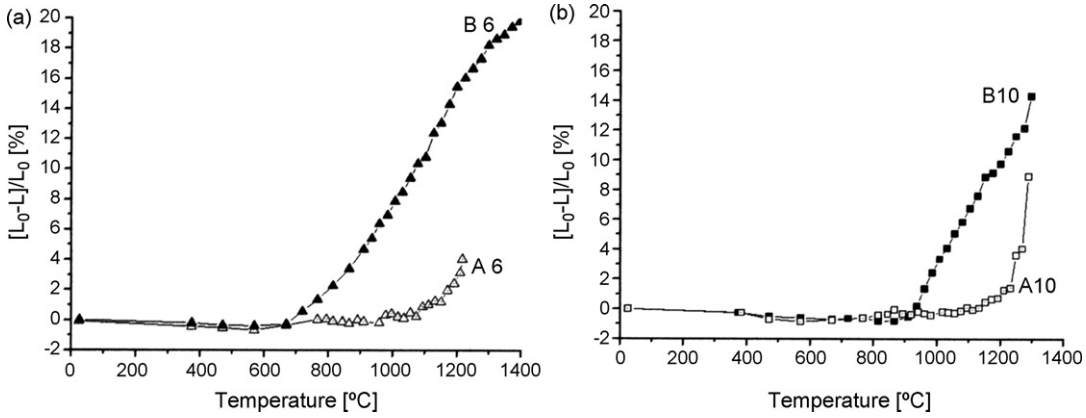

Fig. 2. Shrinkage–temperature curves for A- and B-site compensated PLZT powders. (a) A6/90/10 and B6/90/10; (b) A10/90/10 and B10/90/10.

and A10/90/10 we observed Gaussian particle size distributions; however, for B10/90/10 we observed a bimodal distribution. Hammer et al.[28] also observed a multimodal particle size distribution in PZT 53/47 when excess PbO was used. The excess PbO usually results in liquid phase sintering. It is believed that at the chosen calcination temperature the sintering process starts and as a consequence the agglomerates are formed in the calcined B10/90/10 powder, resulting in a bimodal particle size distribution.

Fig. 2 shows the shrinkage–temperature curves of the calcined A- and B-compensated PLZT powders. From the shape of the curves it is clear that the sintering process is not finished at 1300 °C because the curve is not saturated. This is probably related to the fact that the sintering conditions used in the dynamic sintering experiment, i.e., in shrinkage–*T* curve, were not the same as the static sintering conditions. In the dynamic experiment the samples were not covered with powder of the same composition as during the static sintering. The results based on dynamic experiments clearly show that the onset temperatures for the A-compensated powders are higher than those of the B-compensated powders, i.e., A6/90/10 starts to sinter at 1000 °C, A10/90/10 at 1100 °C, B6/90/10 at 700 °C and B10/90/10 at 850 °C. The onset-of-sintering temperature depends strongly on the initial composition of the powder. It is also clear that the excess PbO shifts the onset temperature to lower values[28] and in a presence of liquid phase the sintering process starts as soon as the liquid phase appears in the particular system.[23] Based on literature data we assume that a PbO-rich liquid phase is present in the B-compensated powders, which enables sintering at lower temperatures compared to sintering in the solid state.[34]

The X-ray powder-diffraction patterns of A6/90/10, B6/90/10, A10/90/10 and B10/90/10 sintered at 1200 °C for 1h in an oxygen atmosphere are shown in Fig. 3. All the diffraction peaks in the A6/90/10 and A10/90/10 patterns belong to the orthorhombic PLZT structure, indexed with PDF 35-739.[33] However, one additional peak with a very low intensity at 29° is observed in the B6/90/10 and B10/90/10 patterns. This peak originates from PbO (PDF 88-1589).[33]

The lattice parameters of the sintered PLZT ceramics were calculated on the basis of an orthorhombic unit cell and are shown in Table 2. The results show that the calculated lattice parameters of A6/90/10 and B6/90/10 as well as A10/90/10 and B10/90/10 have, within the experimental uncertainty, identical values. These findings indicate that the composition of the A- and B-compensated powders does not vary significantly. The calculated lattice parameters for 6/90/10 are slightly higher than those reported in the literature.[29] The difference may be the result of a different heat treatment used during the sintering. Breval et al.[29] sintered pellets at 1325 °C; however, our samples were sintered at 1200 °C. There is, to the best of our knowledge, no published lattice parameter data on PLZT 10/90/10.

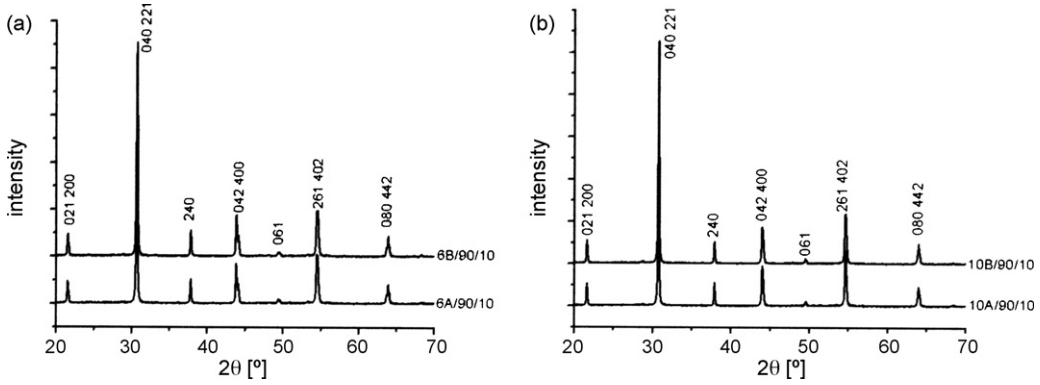

Fig. 3. XRD spectra of PLZT sintered at 1200 °C for 1h in oxygen atmosphere. (a) A6/90/10 and B6/90/10; (b) A10/90/10 and B10/90/10.

Table 2
Calculated unit cell parameters and density of A6/90/10, B6/90/10, A10/90/10 and B10/90/10 sintered at 1200 °C for 1 h in oxygen atmosphere

Sample	Cell parameters (nm)	ρ_T (g/cm^3)	ρ_E (g/cm^3)[a]	ρ_T[a] (%)	Porosity[a] (%)	ρ_E (g/cm^3)[b]	ρ_T[b] (%)	Porosity[b] (%)
A6/90/10	$a = 0.5845 \pm 0.0001$, $b = 1.1690 \pm 0.0003$, $c = 0.8217 \pm 0.0001$	7.8	7.4	95	5	7.49	94	6
B6/90/10	$a = 0.5843 \pm 0.0002$, $b = 1.1689 \pm 0.0003$, $c = 0.8216 \pm 0.0001$	(7.9)	7.7	98	2	7.71	98,8	1,2
A10/90/10	$a = 0.5825 \pm 0.0001$, $b = 1.1645 \pm 0.0003$, $c = 0.8250 \pm 0.0002$	7.7	5.7	74	26	5.9	77	23
B10/90/10	$a = 0.5824 \pm 0.0002$, $b = 1.1640 \pm 0.0003$, $c = 0.8252 \pm 0.0002$	(7.9)	7.4	96	4	7.47	97	3

ρ_E: experimental density, ρ_T: theoretical density.
[a] Density and porosity calculated from mass and dimension of the pellets.
[b] Density and porosity calculated from the microstructure.

The densities of A6/90/10, B6/90/10, A10/90/10 and B10/90/10 calculated from the mass and volume of the pellets together with the amount of porosity calculated from the microstructures (Fig. 4) are shown in Table 2. The percentage of the theoretical density was calculated by dividing the experimental density by theoretical density using the A-site compensation model. The authors are aware that PbO can influence the apparent density by means of mass and dimensions since the PbO have higher density, i.e., 9.67 g/cm^3, than PLZT. For that reason the density calculated from mass and dimensions of the B-compensated pellets should be higher than A-compensated ones. However, in our experiments PbO contribution seems to have insignificant effect on the density value since the density obtained by microstructural analysis and by the mass and dimension of the pellets exhibits within the experimental uncertainty similar values. The value of the porosity obtained from the microstructural analysis, takes into the consideration only the amount of pores and is entirely independent on PbO amount, i.e.,

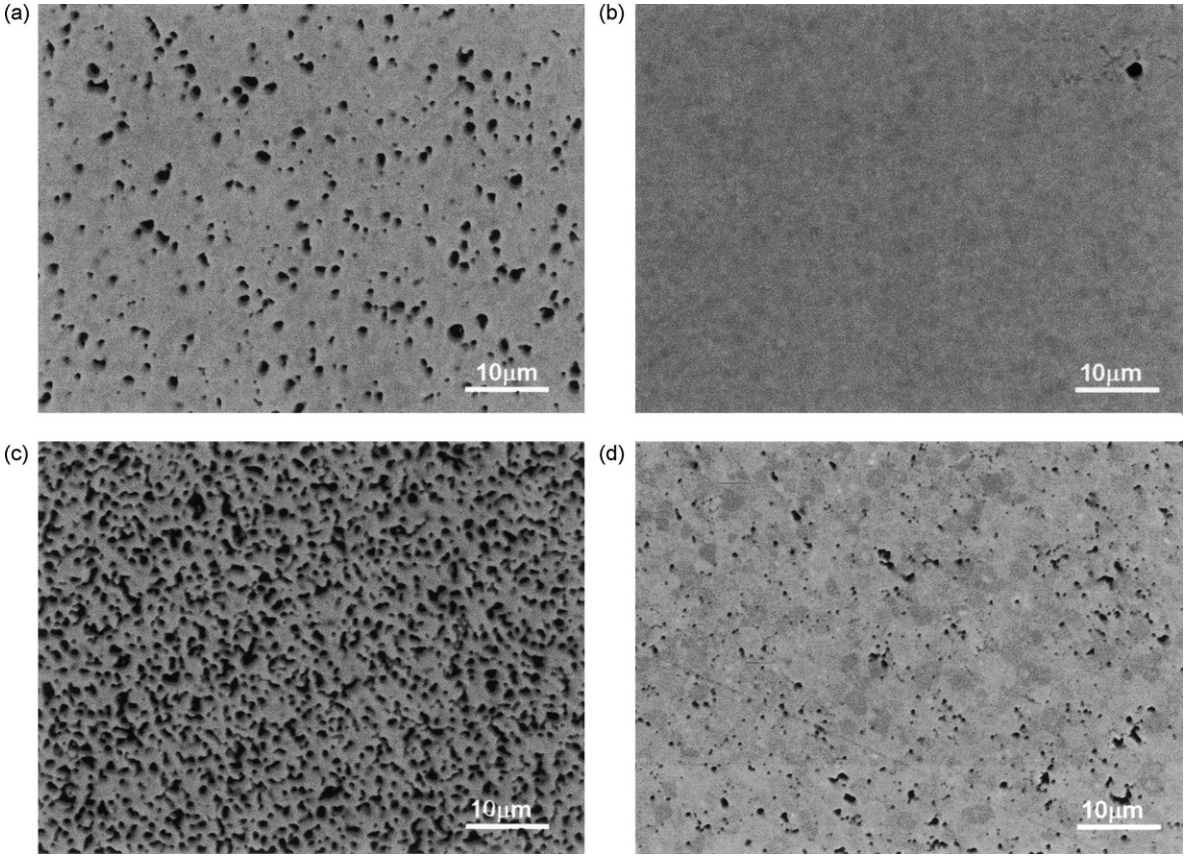

Fig. 4. SEM/BEI images of PLZT sintered at 1200 °C for 1h in oxygen atmosphere. (a) A6/90/10, (b) B6/90/10, (c) A10/90/10 and (d) B10/90/10.

PbO does not play any role in this method. The two independent methods are consistent and show good agreement.

The microstructures of A6/90/10, B6/90/10, A10/90/10 and B10/90/10 sintered at 1200 °C for 1 h in an oxygen atmosphere are shown in Fig. 4. The microstructures of B6/90/10 and B10/90/10 exhibit a lower porosity than the A6/90/10 and A10/90/10 samples. It was also observed that the porosity increases with increasing lanthanum content. These observations are consistent with the calculated densities of these samples, which are shown in Table 2. The highest density, i.e., 7.7 g/cm^3 was calculated for B6/90/10, and the lowest density, i.e., 5.7 g/cm^3, for A10/90/10. A detailed SEM/EDS analysis of these samples showed that the A6/90/10 and A10/90/10 samples contain only the matrix phase, where lead, lanthanum, zirconium and titanium were detected. No secondary phase was observed using this method. However, a secondary phase was detected in the B6/90/10 and B10/90/10 samples. Between the grains containing lead, lanthanum, zirconium and titanium, a bright phase was observed, as shown in Fig. 5. The authors are aware that when analyzing such a small area as the bright phase, the EDS analysis of this phase is not reliable. However, the compositional contrast arises from differences in the local chemical compositions, and the regions with a higher average atomic number appear brighter relative to the regions of lower atomic number. Thus, the bright phase at the grain boundaries can be interpreted as a region with a higher atomic number than that of the grains. Moreover, based on numerous EDS point analysis it was systematically found that the bright phase contains more lead than the grains. From these observations it can be concluded that the B6/90/10 and B10/90/10 samples contain a PbO-rich phase that is segregated in between the PLZT grains, which is in agreement with the literature.[11,12,13,23]

Based on the SEM analysis, the X-ray powder-diffraction and the determination of the unit cell parameters it seems reasonable to believe that the addition of trivalent lanthanum ions to the divalent lead sites in the PLZT 6/90/10 and 10/90/10 structure is, under these experimental conditions, predominantly compensated for by the formation of A-site vacancies. This is in accordance with results published by Park et al.,[35] who found that when lead–zirconate–stanate–titanate with Zr/Ti ratios of 55/15, 66/10 and 66/8 were modified with lanthanum, the charge compensation occurs primarily by the formation of A-site vacancies. It was also reported by Hardtl et al.[2] that the maximum concentration of B-site vacancies decreases with increasing ZrO_2 content. PLZT x/90/10 is zirconium-rich and it seems reasonable to believe that it tends to compensate for the lanthanum addition by the formation of A-site vacancies. We have observed the lead-rich phase in B6/90/10 and B10/90/10 samples (Fig. 5). This observation suggests that the predicted amount of PbO in B-compensated PLZT cannot be incorporated into B6/90/10 nor in the B10/90/10, but it remains in the ceramic as a secondary phase. PbO liquid phase is clearly visible in the microstructure, having a great influence on the densification process. It is noticed in the shrinkage–temperature curves (Fig. 2) that the sintering process in the B6/90/10 and the B10/90/10 powders starts at lower temperatures as a consequence of the presence of excess PbO. In the presence of the PbO-rich liquid phase the sintering process occurs at a 400 °C lower temperature in PLZT B6/90/10 and at a 200 °C lower temperature in PLZT B10/90/10, when compared to the A-compensated PLZT. It is also evident from the microstructures in Fig. 4 that the ceramics containing the PbO-rich phase, i.e., B6/90/10 and B10/90/10, possess fewer pores and reach higher densities when compared to A6/90/10 and A10/90/10. Since PLZT B10/90/10 contains PbO-liquid phase and its onset-of-sintering temperature is lower than that of A10/90/10, we expected even higher density. The reason for the obtained microstructure (Fig. 4d) with non-uniform pore distribution, their shape and consequently lower density is according to our opinion related to the bimodal particle size distribution in calcined B10/90/10 powder. The driving force for densification of material in a presence of liquid phase derived from the capillary pressure of the liquid located between the solid particles. As a result a rearrangement of the particles occur leading to more effecting packaging.[7] As a result the material possesses high density. The improved sintering process of PLZT in the presence of the PbO liquid phase was reported by many authors.[21,23,24,27,28] The presence of liquid phase was not observed in A-compensated PLZT therefore for these samples the main densification mechanism is solid-state sintering as also suggested in the literature.[24,28] From shrinkage–temperature

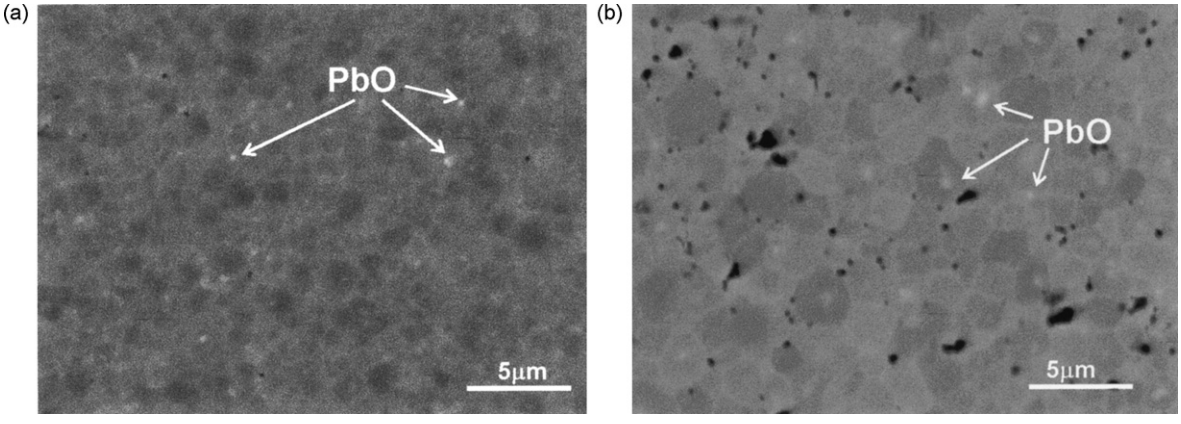

Fig. 5. SEM/BEI image of (a) B6/90/10 and (b) B10/90/10. Between the grains containing lead, lanthanum, zirconium and titanium, the lead-rich phase (denoted as PbO) is identified.

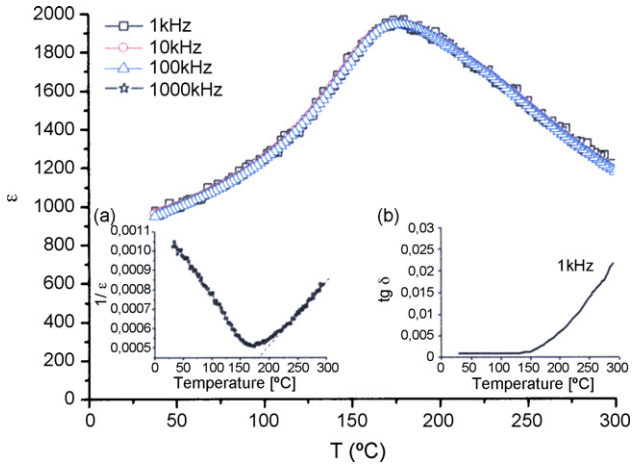

Fig. 6. Temperature dependence of the permittivity ε at 1, 10, 100 and 1000 kHz for A6/90/10 PLZT. The insert shows $1/\varepsilon$ at 1 kHz (graph a) and loss factor tg δ at 1 kHz (graph b).

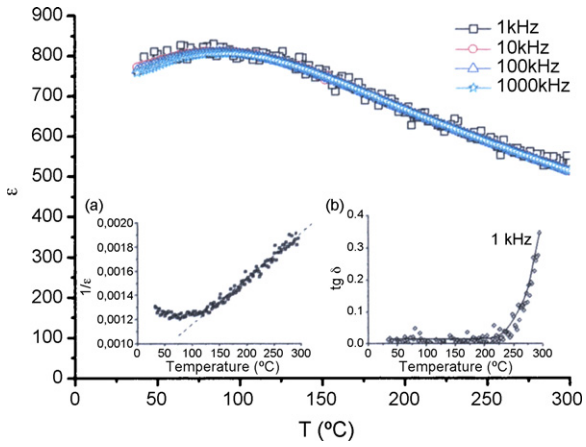

Fig. 8. Temperature dependence of the permittivity ε at 10, 100 and 1000 kHz for A10/90/10 PLZT. The insert shows $1/\varepsilon$ at 1 kHz (graph a) and loss factor tg δ at 1 kHz (graph b).

curves it is obvious that A-compensated samples starts to densify at temperature as high as 1100 °C when the transfer of material can occur by diffusions processes.

Figs. 6–9 show the dielectric response characteristics for A6/90/10, B6/90/10, A10/90/10 and B10/90/10 PLZT, respectively, at 1, 10, 100 and 1000 kHz. In this frequency range the dielectric permittivity of all the samples does not show any noticeable dispersion and is, for the selected sample, practically identical at all frequencies.

The dielectric permittivity for the A6/90/10 and B6/90/10 samples matches over the whole temperature range from 20 to 300 °C. It exhibits a relatively broad maximum with a peak value of 1940 at 176 °C, which is identical for both samples. The insets in Figs. 6 and 7 (graphs a) show the corresponding inverse dielectric permittivity versus temperature. The dielectric constant exhibited a relatively sharp decrease at temperatures below the minimum. At higher temperatures the dielectric constant follows the Curie–Weiss relationship, which is indicated by a straight line (insets a). However, at temperatures slightly higher than 176 °C the deviations from the Curie–Weiss relationship are observed. The graphs (b) shown as insets in Figs. 6 and 7 present the loss factor measured at 1 kHz versus temperature. The loss factor for A6/90/10 and B6/90/10 at 1 kHz does not exceed 0.005 at temperatures up to 150 °C; however, at higher temperatures it increases to a value of 0.03. When the frequency increases the loss factor does not increase so sharply and at 1000 kHz it does not exceed 0.005 at 300 °C. The dielectric characteristics of A6/90/10 and B6/90/10 are identical, indicating that the presence of a small amount of PbO-rich liquid phase at the grain boundaries has an insignificant effect on the dielectric properties of PLZT 6/90/10.

The dielectric permittivities of the PLZTs with the compositions A10/90/10 and B10/90/10, shown in Figs. 8 and 9, exhibit diffused maxima of the dielectric constant, and according to these measurements the phase transformation occurs over a very broad temperature range. The corresponding inverse dielectric permittivities versus temperature, shown as inset (a) in Figs. 8 and 9, indicate that at higher temperatures the dielectric constant follows the Curie–Weiss relationship. The loss-factor values measured at 1 kHz, shown as inset (b), are very low at low

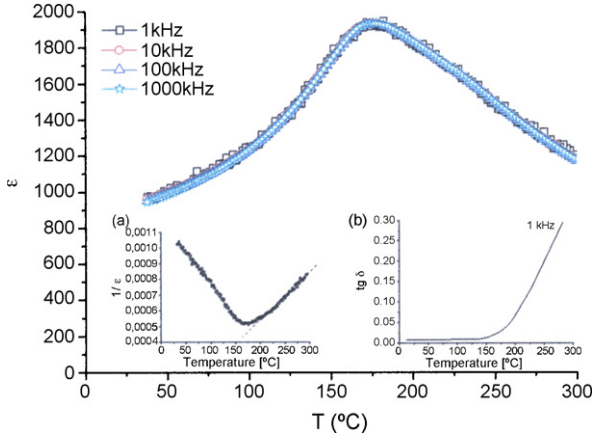

Fig. 7. Temperature dependence of the permittivity ε at 1, 10, 100 and 1000 kHz for B6/90/10 PLZT. The insert shows $1/\varepsilon$ at 1 kHz (graph a) and loss factor tg δ at 1 kHz (graph b).

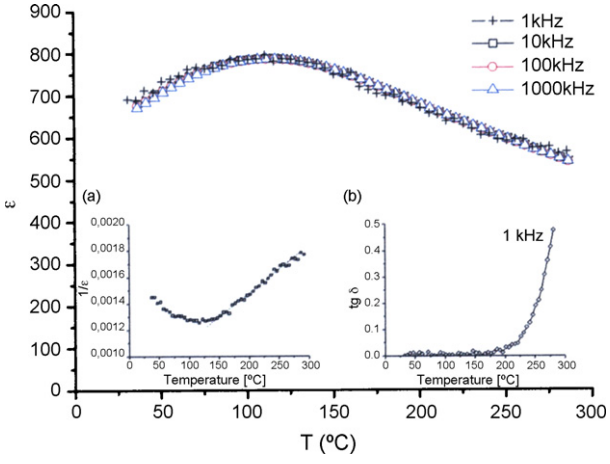

Fig. 9. Temperature dependence of the permittivity ε at 1, 10, 100 and 1000 kHz for B10/90/10 PLZT. The insert shows $1/\varepsilon$ at 1 kHz (graph a) and loss factor tg δ at 1 kHz (graph b).

temperatures; however, at higher temperatures they markedly increase. The loss factor apparently increases at temperatures above 250 °C for A10/90/10, reaching a value of 0.35 at 280 °C. For B10/90/10 it starts to increase at lower temperatures, i.e., at 200 °C and reaches a value of 0.45 at 280 °C. The increase in the loss factor is the most noticeable at a frequency of 1 kHz and decreases considerably with increasing frequency. Based on these experimental observations we believe that the loss factor increases at high temperatures and low frequencies due to dc conductivity.

According to the published PLZT phase diagrams,[29,30] PLZT with the composition 6/90/10 is an antiferroelectric phase, while PLZT 10/90/10 should be a mixture of orthorhombic PLZT and pyrochlore $La_2Zr_2O_7$. Our results show that A6/90/10, B6/90/10, A10/90/10 and B10/90/10 do not contain any $La_2Zr_2O_7$ phase and crystallize in the orthorhombic perovskite structure. To find out whether 6/90/10 and 10/90/10 exhibit antiferroelectric behavior, as suggested in the literature, the hysteresis loops were measured. Since in the literature the double hysteresis loops for PZT and PLZT were observed at an electric field of 40 kV/cm[1], the double hysteresis loops were not observed for any of our samples, even at very high electric fields of 100 kV/cm. Based on these observations we have no clear evidence that any of our samples is an antoferroelectric phase at room temperature. To clarify this, further analyses are planned.

4. Conclusions

It was shown that the relevant differences between A-site compensated lead–lanthanum–zirconium–titanate, i.e., $Pb_{1-3x/2}La_x(Zr_{0.9}Ti_{0.1})O_3$ and B-site ones, i.e., $Pb_{1-x}La_x(Zr_{0.9}Ti_{0.1})_{1-1x/4}O_3$, is the sintering mechanism and the microstructural characteristics.

A- and B-compensated PLZT x/90/10 ceramics with $x = 0.06$ and 0.10 were prepared by processing the ceramics under identical experimental conditions, i.e., at 1200 °C in an oxygen atmosphere. The PLZT ceramic under investigation possesses an orthorhombic structure. The lattice parameters of the A- and B-compensated PLZT are, within the experimental uncertainty, the same, indicating that the compositions of the A- and B-compensated ceramics do not vary significantly.

B-compensated PLZT powders start to densify at lower temperatures and possess higher densities than the A-compensated powders. The PbO-rich liquid phase that was detected in the B-compensated powders segregates at the grain boundaries and enables liquid phase sintering. A-compensated PLZT start to densify at temperatures as high as 1100 °C and the suggested mechanism is solid-state sintering.

The permittivity versus temperature measurements of PLZT 6/90/10 and 10/90/10 show that in the frequency range from 1 to 1000 kHz the dielectric permittivities of all the samples do not show any dispersion and are, for the selected samples, identical. PLZT 6/90/10 exhibits a phase transition at 176 °C; however, PLZT 10/90/10 exhibits a phase transformation over a broad temperature range. At high temperatures the dielectric constant follows the Curie–Weiss relationship, but at the transition temperature there is a clear deviation from this relationship. The loss factor increases with increasing temperature and decreases with increasing frequency, which is a consequence of the dc conductivity in the PLZT material.

Out results indicate that the charge neutrality in PLZT 6/90/10 and 10/90/10 occurs predominantly by the formation of A-site vacancies. The lead-rich liquid phase in the B-compensated PLZT enables sintering at 200 to 400 °C lower temperatures than the A-compensated PLZT and leads to higher densities of the ceramic. The dielectric response characteristics of the A- and B-compensated PLZT are comparable, indicating that a small amount of PbO liquid phase does not deteriorate the dielectric permittivity of PLZT.

Acknowledgments

This research was supported by the MC Fellowship Association CERAMOS (HPMT-CT-2001-00372). Mr. Silvo Drnovšek, Mrs. Jena Cilenšek and Mrs. Katja Štajner are acknowledged for technical assistance and dr. Vid Bobnar for valuable discussions.

References

1. Viehland, D., Li, J.-F., Dai, X. and Xu, Z., Structural and property studies of high Zr-content lead zirconate titanate. *J. Phys. Chem. Solids*, 1996, **57**, 1545–1554.
2. Hardtl, K. H. and Hennings, D., Distribution of A-site and B-site vacancies in (Pb,La) (Ti Zr)O_3 ceramics. *J. Am. Ceram. Soc.*, 1972, **55**(5), 230–231.
3. Holman, R. L., The defect structure of 8/65/35 PLZT as determined by Knudsen effusion. *Ferroelectrics*, 1976, **10**, 185–190.
4. Hennings, D. and Hardtl, K. H., Distribution of vacancies in lanthana-doped lead titanate. *Phys. Stat. Sol. (a)*, 1970, **3**, 465–474.
5. Heartling, G. H., In *Electronic Ceramics*, ed. L. M. Levinson. Marcel Dekker, New York, 1988, pp. 371–492.
6. Hardtl, K. H. and Rau, H., PbO vapour pressure in the $Pb(Ti_{1-x}Zr_x)O_3$ system. *Solid State Commun.*, 1969, **7**, 41–45.
7. Kingery, W. D., Bowen, H. K. and Uhlman, D. R., *Introduction to Ceramics*. John Wiley & Sons, New York, 1976.
8. Rossetti, G., Rodriguez, M. A., Navrotsky, A., Cross, L. E. and Newnham, R. E., Structure of the defect perovskite $(Pb_{0.85}La_{0.1})TiO_3$ between 10 and 1023 K. *J. Appl. Phys.*, 1995, **77**(4), 1683–1689.
9. Hennings, D., The range of existence of perovskite phases in the system. *Mater. Res. Bull.*, 1971, **6**(5), 329–339.
10. Snow, G. S., Improvements in atmosphere sintering of transparent PLZT ceramics. *J. Am. Ceram. Soc.*, 1973, **56**(9), 479–480.
11. Snow, G. S., Fabrication of transparent electrooptic PLZT ceramic by atmosphere sintering. *J. Am. Ceram. Soc.*, 1973, **56**(2), 91–96.
12. Northrop, D. A., Vaporization of lead zirconate-lead titanate materials. *J. Am. Ceram. Soc.*, 1967, **50**(9), 441–445.
13. Polli, A. D., Lange, F. F. and Levi, C. G., Metastability of the fluorite, pyrochlore and perovskite structure in the PbO–ZrO_2–TiO_2 system. *J. Am. Ceram. Soc.*, 2000, **83**(4), 879–881.
14. Matsuo, Y. and Sasaki, H., Formation of lead zirconate–lead titanate solid solutions. *J. Am. Ceram. Soc.*, 1965, **48**, 289–291.
15. Hankey, D. L. and Biggers, J. V., Solid-state reactions in the system PbO–TiO_2–ZrO_2. *J. Am. Ceram. Soc.*, 1981, **64**, C172–C173.
16. Chandratreya, S. S., Fulrath, R. M. and Pask, J. A., Reaction mechanisms in the formation of PZT solid solutions. *J. Am. Ceram. Soc.*, 1981, **64**, 422–425.
17. Hiremath, B. V., Kingon, A. I. and Biggers, J. V., Reaction sequence in the formation of lead zirconate–lead titanate solid solution: Role of raw materials. *J. Am. Ceram. Soc.*, 1983, **66**, 790–793.
18. Venkataramani, S. and Biggers, J. V., Reactivity of zirconia in calcining of lead zirconate–lead titanate compositions prepared from mixed oxides. *Ceram. Bull.*, 1980, **59**, 462–466.

19. Holman, R. L. and Fulrath, R. M., Intrinsic nonstoichiometry in the lead zirconate–lead titanate system determined by Knudsen diffusion. *J. Appl. Phys.*, 1973, **44**, 5227–5236.
20. Kingon, A. I. and Clark, J. B., Sintering of PZT ceramics: I. Atmosphere control. *J. Am. Ceram. Soc.*, 1983, **66**(4), 253–256.
21. Kingon, A. I. and Clark, J. B., Sintering of PZT ceramics: II. Effect of PbO content on densification kinetics. *J. Am. Ceram. Soc.*, 1983, **66**(4), 256–260.
22. Bernik, S., Marinenko, R. B., Holc, J., Samardžija, Z., Čeh, M. and Kosec, M., Compositional homogeneity of ferroelectric (La,Pb) (Zr Ti)O_3 thick films. *J. Mater. Res.*, 2003, **18**(2), 512–523.
23. Kosec, M., Kolar, D. and Stojanovic, B., Effect of excess PbO on the properties of PLZT ceramics. In *High Tech Ceramics*, ed. P. Vincenzini. Elesevier, Amsterdam, 1987, pp. 2127–2134.
24. Kong, L. B., Ma, J., Zhang, R. F. and Zhang, T. S., Fabrication and characterisation of lead lanthanum zirconata titanate (PLZT 7/40/60) ceramics from oxides. *J. Alloys Compd.*, 2002, **339**, 167–174.
25. Kosec, M., Effect of lead content on structure and properties of lead based ceramic dielectrics. *Sci. Sintering*, 1995, **26**(1), 21–27.
26. Kosec, M., Holc, J., Malič, B. and Bobnar, V., Processing of high performance lead lanthanum zirconate titanate thick films. *J. Eur. Ceram. Soc.*, 1999, **19**(6–7), 949–954.
27. Lin, W. K. and Chang, Y. H., Behaviour of PbO in the two-stage sintering of PLZT ceramics. *Mater. Sci. Eng. A*, 1994, **186**, 177–183.
28. Hammer, M. and Hoffman, M. J., Sintering model for mixed-oxide-derived lead zirconate titanate ceramics. *J. Am. Ceram. Soc.*, 1998, **81**(12), 3277–3284.
29. Breval, E., Wang, C. and Dougherty, J. P., PLZT phases near lead titanate. I. Determination by X-ray diffraction. *J. Am. Ceram. Soc.*, 2005, **88**(2), 437–442.
30. Heartling, G. H., Ferroelectric ceramics: History and technology. *J. Am. Ceram. Soc.*, 1999, **82**(4), 797–818.
31. Xu, Z., Dai, X. and Viehland, D., Incommensuration in La-modified antiferroelectric lead zirconate titanate ceramics. *Appl. Phys. Lett.*, 1994, **65**(25), 3287–3289.
32. Zhang, W., Huebner, W., Sampayan, S. E. and Krogh, M. L., Polarization switching of and electron emission from lead lanthanum zirconate titanate ceramics. *J. Am. Ceram. Soc.*, 1999, **82**(3), 591–599.
33. PDF-ICDD. PCPDFWin Version 2.2, June 2001. International Centre for Diffraction Data, 2002.
34. Atkin, R. B. and Fulrath, R. M., Point defects, sintering of lead zirconate–titanate. *J. Am. Ceram. Soc.*, 1971, **54**, 265–270.
35. Park, S. E., Markowski, K., Yoshikawa, S. and Cross, L. E., Effect on electrical properties of barium and strontium additions in the lead lanthanum zirconate stannate titanate system. *J. Am. Ceram. Soc.*, 1997, **80**(21), 407–412.